Signal Variation in Single Particle Aerosol Mass Spectrometry

by

Zachary Daniel Wissner-Gross

Submitted to the Department of Physics
in partial fulfillment of the requirements for the degree of

Bachelor of Science in Physics

at the

MASSACHUSETTS INSTITUTE OF TECHNOLOGY

June 2007

Author .....
Department of Physics
May 11, 2007

Certified by .....
Matthias Frank
Principal Investigator, LLNL
Thesis Supervisor

Certified by .....
Young Lee
Associate Professor
Thesis Supervisor

Accepted by .....
David E. Pritchard
Thesis Coordinator

Signal Variation in Single Particle Aerosol Mass Spectrometry

by

Zachary Daniel Wissner-Gross

Submitted to the Department of Physics
on May 11, 2007, in partial fulfillment of the
requirements for the degree of
Bachelor of Science in Physics

Abstract

Rapid and accurate detection of airborne micro-particles is currently an important problem in national security. One approach to such detection, bioaerosol mass spectrometry (BAMS), is currently under development at Lawrence Livermore National Laboratory. BAMS is a type of single particle aerosol mass spectrometry that rapidly records dual-polarity mass spectra of aerosolized micro-particles. However, the accuracy of the BAMS system is limited by various uncertainties, resulting in shot-to-shot variations in the mass spectra. I found that the variations in mass peak areas in BAMS spectra were significantly larger than those predicted by Poisson statistics based on the mean number of detected ions. Furthermore, these variations were surprisingly consistent as a function of peak area among synthetic, organic, and biological samples. For both positive and negative ions, the standard deviation in a peak's area was approximately proportional to the mean value of that area to the 0.9 power. Using the consistency of this data, I also developed a novel method for quantitatively evaluating the similarity between mass spectra using a chi-square factor. Peak area variations in other single particle aerosol mass spectrometers may be similarly analyzed and used to improve methods for rapid particle identification.

Thesis Supervisor: Matthias Frank
Title: Principal Investigator, LLNL

Thesis Supervisor: Young Lee
Title: Associate Professor

Acknowledgments

The development of the BAMS system at LLNL was funded through DARPA and TSWG by the Department of Defense. This work was performed under the auspices of the U.S. Department of Energy (DOE) by University of California, Lawrence Livermore National Laboratory under Contract W-7405-ENG-48. I performed this research while on appointment as a U.S. Department of Homeland Security (DHS) Scholar under the DHS Scholarship and Fellowship Program, administered by the Oak Ridge Institute for Science and Education (ORISE) for DHS through an interagency agreement with DOE. ORISE is managed by Oak Ridge Associated Universities under DOE contract number DE-AC05-06OR23100. All opinions expressed in this paper are the author's and do not necessarily reflect the policies and views of DHS, DOE, or ORISE.

I would like to thank Young Lee for his valuable comments on this work. I am most grateful to George R. Farquar, Paul T. Steele, Audrey N. Martin, Michael J. Bogan, Elisabeth A. Wade, Herbert J. Tobias, David P. Fergenson, and Matthias Frank, my colleagues at LLNL who helped in every aspect of this project.

Finally, I would like to thank my family: Liz, Sig, Alex, and Winnie. Throughout my education, I have been continually blessed with their constant support.

Contents

Chapter 1

Introduction

1.1 Mass Spectrometry

Mass spectrometry is a technique commonly employed in analytical chemistry, biology, and physics for the identification of a variety of samples, ranging from metal isotopes to entire proteins. In mass spectrometry, individual molecules and/or their fragments are ionized by one of several methods, such as electrospray and laser desorption/ionization (LDI), after which the resulting ions are separated by their mass-to-charge ratio. The two most common techniques for ion separation are through orthogonal electric and magnetic fields, and time-of-flight mass spectrometry (TOF-MS).

When an ion with mass m and charge q is accelerated through an electric potential U into a chamber with orthogonal electric and magnetic fields E and B respectively, such that both fields are also orthogonal to the initial velocity of the ion, then the ion will travel linearly through the chamber to a detector if it has a specific mass-to-charge ratio:

$$\frac{q}{m} = \frac{1}{2U}\left(\frac{E}{B}\right)^2 \tag{1.1}$$

In TOF-MS, the ion is again accelerated through a potential U, but now into a flight tube of length d with no internal electromagnetic fields. If the ion requires a time t

to reach the detector, then its mass-to-charge ratio is:

$$\frac{q}{m} = \frac{1}{2U}\left(\frac{d}{t}\right)^2 \tag{1.2}$$

Time-of-flight mass spectrometry allows for the simultaneous measurement of all ions generated, since they all reach the detector in an ideal system.

1.2 Single Particle Aerosol Mass Spectrometry

Single particle aerosol mass spectrometry (SPAMS) is used to identify the composition of single particles based on the presence of specific ionic markers in their mass spectra [1]. Using SPAMS, matrix-assisted laser desorption/ionization (MALDI) mass spectrometry, or other forms of mass spectrometry, different samples can be distinguished by analyzing both which markers are present and by comparing the relative peak heights or areas of those markers, which together constitute a characteristic "fingerprint," or "pattern." Uncertainty in the positions and areas of these peaks reduce the precision of mass spectral differentiation. To my knowledge, such uncertainty has not been thoroughly examined in SPAMS until now.

In this study, a specific type of SPAMS was used, known as bioaerosol mass spectrometry (BAMS), which is currently being developed at Lawrence Livermore National Laboratory (LLNL). BAMS is a form of laser desorption/ionization time-of-flight mass spectrometry (LDI-TOFMS) that operates in real time to detect aerosolized micrometer-sized particles (with or without sample preparation), and has been shown to detect trace sample concentrations as low as 14 zmol [2]. To date, the BAMS device has successfully detected biological agents and high explosives [3]. Here BAMS was used as a representative method of SPAMS, featuring dual-polarity mass spectra and aerodynamic particle sizing [1, 4].

The variation in SPAMS peak area is due to variation in both the number of ions that reach the detector and in the detector's response. Error introduced by the digital-to-analog conversion process was found to be negligible. Variation in the response of

the detector, which in the case of BAMS consists of two microchannel plates (MCPs) in a chevron formation, can be determined by observing its response to single ions. Determining th enumber of ions that reach the detector per aerosolized micro-particle, along with the uncertainty in that number, is a more difficult matter. A fraction of the molecules within each (not necessarily homogeneous) particle is ionized by a laser pulse that is not perfectly uniform in space or time [5, 6]. Furthermore, ionization efficiency is highly specific to the type of molecule in study, its preparation [7], and the SPAMS system [8], and individual ionization events may not be independent [1, 9]. Finally, not all ions generated during the LDI process reach the detectors. In an ideal system, each particle is identical in size and composition, and its constituent molecules are ionized under identical conditions. In the event that each particle contains the same number of molecules of each species, and that for a given species (or molecular fragment) the probability of ionization and detection of every molecule is the same, the number of ions of each species detected per particle would follow a Poisson distribution. The total recorded mass spectrum signal per particle has been observed in a MALDI ion trap system, and the distribution does not appear Poisson [10]. Nevertheless, a Poisson distribution of ions represents an ideal lower limit in uncertainty.

In this study, the gain curve of the MCP detector was determined by attaching an ion gauge to the TOF-MS chamber. Ions created by the gauge entered the chamber, and these ions underwent essentially the same acceleration toward the MCP detectors as ions from laser desorbed/ionized micro-particles. The observed distribution in single ion response was then used to construct a theoretical lower bound on the uncertainty in mass peak areas. Next, the spectra of synthetic, organic, and biological samples were acquired and their peak area variations were compared to the theoretical limit. Finally, the variations among entire spectra were compared via a chi-square factor, offering a new technique for quantitatively determining the similarity between spectra. While this work was performed using BAMS, it pertains to all other SPAMS techniques as well.

Chapter 2

Theory

Two sources of uncertainty in mass spectrum peak area lie in the number of ions that reach the detector and in the single ion response of the detector. Suppose a given signal from the MCP, y, is the sum of n single ion responses, which follow a distribution of mean R and standard deviation σ_r. For a given particle, suppose the distribution for n has mean N and standard deviation σ_n. It can be shown that the uncertainty in y is then [11]:

$$\sigma_y = \sqrt{N\sigma_r^2 + R^2\sigma_n^2}. \tag{2.1}$$

While R and σ_r can be determined from the MCP's single ion response distribution, and

$$N \approx \frac{\langle y \rangle}{R}, \tag{2.2}$$

determining σ_n is more difficult.

The simplest model for the distribution of the number of ions generated and detected per aerosol particle is Poissonian ($\sigma_n = \sqrt{N}$). In this case, Equation 2.1 simplifies to

$$\sigma_y = \sqrt{N(\sigma_r^2 + R^2)}. \tag{2.3}$$

Combining Equations 2.2 and 2.3 yields

$$\sigma_y = c_r\sqrt{\langle y \rangle}; c_r = \sqrt{\frac{\sigma_r^2 + R^2}{R}}. \tag{2.4}$$

The uncertainty in signal is proportional to the square root of the average signal, and the constant of proportionality depends solely on the mean and standard deviation of the single ion response. Equation 2.4 represents a fundamental lower limit in signal uncertainty. In practice, σ_n is significantly larger than $\sqrt{N}$. There has been discussion in recent years regarding the distribution of ions generated per particle in laser desorption/ionization TOF-MS, and it does not appear Poissonian [10, 12, 9].

Previously, mass spectra were compared by converting them to mutli-dimensional vectors and calculating the angular separation between them using a dot product [13]. In a comprehensive study, Stein and Scott ranked five different metrics for search algorithms that compared mass spectra, finding that the angular separation proved the best metric among them [14]. However, with the knowledge of uncertainties in each peak height, such differences among spectra can now be quantified via a chi-square value. Given a variable mass spectrum vector $\vec{Y} = (y_1, y_2, \ldots, y_k)$ and a reference mass spectrum vector $\vec{Z} = (z_1, z_2, \ldots, z_k)$, the reduced chi-square value for $\vec{Y}$ with respect to $\vec{Z}$ is:

$$\chi_\nu^2 = \frac{1}{k}\sum_{i=1}^{k}\frac{(y_i - z_i)^2}{\sigma_{z_i}^2}. \tag{2.5}$$

If Equation 2.4 applies, then the reduced chi-square value further simplifies to

$$\chi_\nu^2 = \frac{1}{kc_r^2}\sum_{i=1}^{k}\frac{(y_i - z_i)^2}{z_i^2}. \tag{2.6}$$

A reduced chi-square value near unity would indicate that the variation between the measured spectrum and the expected spectrum could be explained statistically. If the reduced chi-square value is much larger than one, other reasons for variation likely exist (e.g., biological differences between samples or a severe lack of uniformity in the LDI process).

Chapter 3

Materials and Methods

3.1 The BAMS Device

The BAMS device, shown in Figure 3-1, has been previously described elsewhere [13]. It consists of both a mass spectrometer and in-house software for the analysis of spectra. Micrometer-sized aerosol particles are generated in a Collison salter nebulizer (BGI Inc., CN-25,27), after which they are passed through a silicon diffusion drier to remove moisture. The particles then arrive at the converging nozzle and pressure flow reducer, where they are focused to the center of the device by an aerodynamic focusing lens. Upon reaching terminal velocity, the particles scatter the light of three or more tracking lasers (CW, 660 nm). The scattered light from these lasers is detected by photomultiplier tubes, and the times of the scattering events are recorded to calculate the particle velocity, from which the aerodynamic diameter is determined. At the appropriate time, the system triggers a desorption/ionization Q-switched frequency-quadrupled Nd:YAG laser (Ultra CFR, Big Sky Laser Technologies, Inc.), operating at 266 nm with 7 ns (FWHM) pulses. Prior to ionization, the laser pulse passes through an aperture, a half-wave plate, a polarizer, and a 10 cm plano-convex lens, which focus the pulse to a cross-sectional diameter of approximately 330 μm and appropriately attenuate its energy. Positive and negative ions are generated via the interaction between the pulse and the particles, and these ions are simultaneously accelerated in opposite directions in the TOF-MS chamber. The ions are redirected and focused

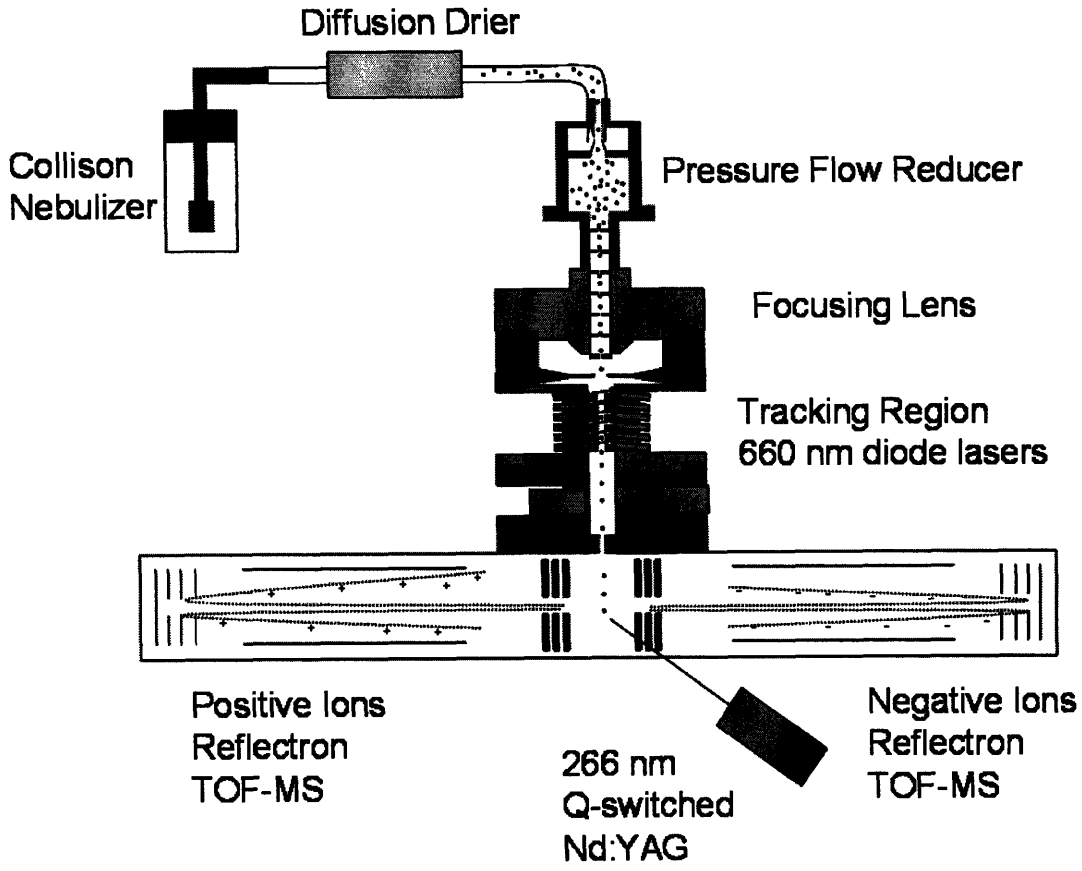

Figure 3-1: Schematic of the BAMS device.

by reflectrons and ultimately impact two sets (one for positive ions, and one for negative ions) of MCP detectors (Burle Technologies, Inc.) in chevron formation. The gains of the MCPs were not expected to be mass- or velocity-dependent, as they were operated at voltages sufficient for space-charge saturation [15]. The MCP outputs were converted to an 8-bit scale with a variable gain setting by an 8-bit analog-to-digital digitizer with 2 ns resolution (Signatec PDA 1000). A constant set of voltage settings was used for the TOF-MS ion optics and detectors. The most relevant voltages were the biases between the fronts and backs of the MCP detectors. The bias in the MCP detecting positive ions was 1838 V; the bias in the MCP detecting negative ions was 1773 V.

3.2 Single Ion Generation and Detection

Single ions were generated by attaching an ion gauge (Nor-Cal 4336K) to the dual-polarity TOF-MS chamber of the BAMS device. Pressure in the chamber was typically less than 1×10^{-6} Torr. Electrons were directly released from the gauge filament and accelerated into the chamber, and other heavier ionic species were generated through the collisions between electrons and gas molecules. The output of each MCP was sent to a DC-coupled 500 MHz 20 dB (10×) amplifier with a 50 Ω input impedance (FEMTO HVA-500M-20-B), and then to a digital oscilloscope (Tektronix TDS 7104). Pulses caused by ion collisions at both MCPs were generally several millivolts in amplitude and lasted several nanoseconds. The trigger setting used for the oscilloscope was different for the two MCPs: for positive ions the trigger was 16.0 mV, after 10× amplification; for negative ions, the trigger was 18.8 mV after amplification.

For each polarity, 10,000 triggered events were recorded, containing the amplified voltages from 20 ns before to 30 ns after each triggered event, with 500 data points spread over the 50 ns. Figure 3-2a shows typical positive and negative ion pulses. Each had a characteristic shape: pulses from the positive ion MCP comprised a large negative peak, followed by several weaker peaks of alternating sign; pulses from the negative ion MCP contained several "fingers," or negative peaks about 2 ns apart. These shapes were likely the result of the properties of the signal conditioning and biasing electronics of the two different MCPs. The first 15 ns of each pulse spectrum were averaged to zero. If the absolute value of the voltage in the first 15 ns or final 10 ns of any spectrum ever exceeded 2 mV, that spectrum was thrown out. After this initial qualification, 9855 positive spectra and 9946 negative spectra were used for further analysis.

While acquiring spectra, he BAMS digitizer recorded the MCP output every 2 ns. One Dalton in the mass spectrum generally corresponded to a few hundred ns, while single ion pulses were only several ns long. The digitizer therefore too k "snapshots" of the summed responses to a number the ions, and the area of a peak in the mass spectrum approximately equaled the sum of the single ion responses.

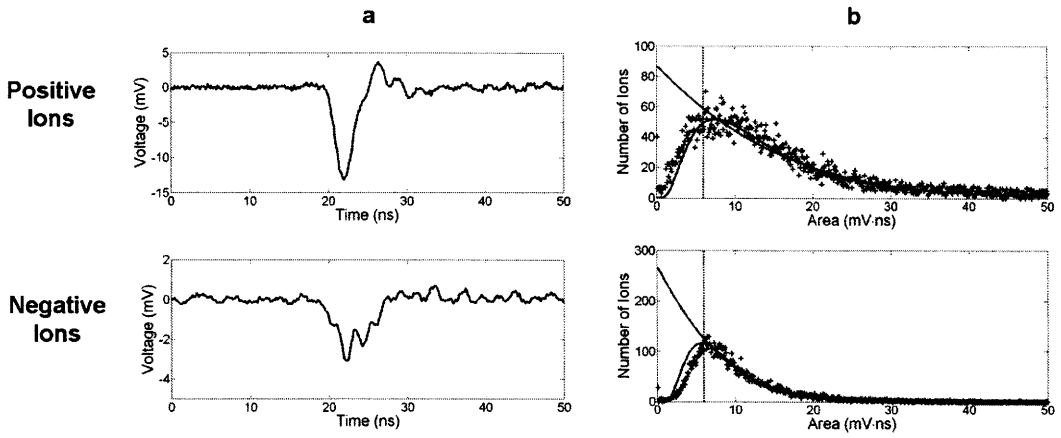

Figure 3-2: Single ion response of the MCP detectors. a) Typical response of the positive and negative ion MCP detectors without amplification. b) Pulse area distribution of the positive and negative ion MCPs with a bin size of 0.1 mV·ns. Both Gaussian (upper fit) and log-normal (lower fit) distributions were fitted to the data right of the vertical dotted line, located at 6 mV·ns.

3.3 Sample Preparation and Data Acquisition

Four separate aerosol samples were prepared for BAMS analysis: polystyrene latex (PSL) spheres with a 1.0 μm diameter, PSL spheres with a 3.0 μm diameter, a mixture of arginine and dipicolinic acid (arginine-DPA), and *Bacillus atrophaeus* spores. Both sets of spherical PSLs (Duke Labs) were stored in water, and approximately 5 mL of each PSL mixture was poured into nebulizers for aerosolization and BAMS analysis. The arginine-DPA sample was prepared by dissolving 188 mg of L-arginine MonoHCl (Research Plus Inc., Bayonne, NJ) and 180 mg of DPA (Aldrich) in 200 mL of deionized water. The mixture was sonicated for 5 minutes, and then 5 mL was transferred to a nebulizer for aerosolization. The spore sample was grown at LLNL.

For each sample, the same ion optics and MCP detector voltage settings were used as in the MCP single ion response study, so that the theoretically derived lower limit of peak area variation in Equation 2.4 could be directly compared to experimental results. The mass spectra of approximately 3000 microparticles hit by the desorption/ionization laser beam were recorded for each of the four samples. For each sample, 1000 mass spectra were recorded for each of three different gain settings on

the digitizer, in which 256 bits were equivalent to 333 mV, 1.8 V, or 3.0 V. The different gain settings were used to study different mass peaks, some of which saturated the lower settings or were too small for the higher settings. Comparable baseline and trigger settings were used for each sample and at each gain setting. Mass spectra were calibrated using the previously observed peaks of the arginine-DPA spectrum.

Different laser fluences were used for the different samples because the fluence drifted over the course of experimentation: 1 μm PSLs were ionized with a laser energy of 656 $\pm$ 21 μJ over the 330 μm diameter beam; 3 μm PSLs were ionized with an energy of 686 $\pm$ 8 μJ, and both arginine-DPA and the spores were ionized with an energy of 254 $\pm$ 26 μJ.

Chapter 4

Results and Discussion

4.1 Single Ion Response

In an MCP detector, ions eject secondary electrons upon impact that cascade through the channel, resulting in a typical overall gain on the order of 10^3-10^4. Each step in the cascade likely has the same gain distribution. However, the shape of this distribution is not known, and therefore the expected shape of the overall gain distribution is not known. Several studies have examined the shape of the MCP pulse height distribution, and a common fitting is a Gaussian, or truncated Gaussian, distribution. Furuya and Hatano fitted a Guassian with slightly different widths on either side of the mode to their pulse height data [16]. Studying an Al_2O_3 surface at sub-saturating voltages, Axelsson et al. also fitted their secondary electron count distribution with a Gaussian function [17]. Hunter and Streseau used a Poisson distribution, but dealt exclusively with Monte Carlo simulations and did not report any experimental data [18]. Cohen et al. conducted an intriguing study in which they assumed different gain distributions in the individual cascading steps within an MCP and modeled the result using the theory of branching processes [11]. While a Poisson distribution visually appeared to accurately represent their experimental data, they determined that a log-normal distribution was a better fit.

The pulse area distribution (Figure 3-2b) was used to determine the statistics of the MCP single ion response. However, this distribution was incomplete because

Table 4.1: Mean and standard deviation of the MCP single ion response in the BAMS device for both positive and negative ions.

Ions	MCP Bias (V)	R (mV·ns)	σ_r (mV·ns)
Positive	1838	13.7 ± 2.9	11.5 ± 1.5
Negative	1773	7.5 ± 2.2	5.2 ± 0.1

pulses with amplitude less than 2 mV were not adequately detected by the oscilloscope. Therefore, only pulses with areas larger than 6 mV·ns were fitted. The two functional fits used were a Gaussian and a log-normal distribution. The means and standard deviations of the two fits were combined, giving a range on the statistics of single ion response. The resulting values for R and σ_r for both positive and negative ions are shown in Table 4.1. Accounting for the missing lower-amplitude pulses by the fitting of the higher-amplitude data effectively lowered the mean of the pulse area distribution by approximately 16 percent for positive ions and 24 percent for negative ions.

4.2 Variation in Peak Heights

A number of mass peaks were identified in the spectra of PSLs, the arginine-DPA, and the spore samples. Depending on the height of peak, its area was recorded using an appropriate gain setting so that peak height was maximized without saturation. The measured peaks are shown in Figure 4-1. These peaks represent a variety of different ions: while some are simple cations or anions found in the sample's preparation solution (such as mass peak +39, which is K^+), others represent more complex molecules found only in the micro-particles (such as -122 in the spore and arginine-DPA spectra, which is DPA-CO_2H). But for each peak, the distribution of ions per particle should be limited by Poissonian statistics, and the variation should be greater than that given by Equation 2.4.

The distributions in area for each of these peaks are shown in Figure 4-1. The areas clearly do not follow a Poisson distribution; instead, they are generally spread over

a range that is twice the average. The distributions also exhibit one of two general shapes: often there is a maximum at or near zero and then another local maximum at some larger value (e.g., +51 and -49 from the PSLs); otherwise, there is a single maximum with a positive skewness (e.g., the arginine-DPA peaks and +122 from the spores). Figure 4-2 shows a comparison between the peak area distribution for one of the mass peaks (+129 from the 1 μm PSL spectrum) and the distribution predicted by combining the single ion response from Figure 3-2b with Poissonian statistics for the number of ions generated per micro-particle. The model curve represents the average of twenty-five Monte Carlo simulations. The peak at +129 was relatively small, and each micro-particle generated on average about sixty of these ions. Thus, while the modes of the two distributions in Figure 4-2 are significantly offset, their widths are comparable. Some of the larger peaks in the mass spectra consisted on average of hundreds or even thousands of ions. For these peaks, the model distributions were much narrower about the mean peak area than the observed peak area distributions were.

The mean and standard deviation for each of the distributions in Figure 4-1 were calculated, and these results are shown in Figure 4-3. The variation in peak area for each sample was approximately an order of magnitude larger on average than the Poissonian lower limit. Surprisingly, the trend of peak area versus variation seems independent of the sample. The synthetic, organic, and biological samples all lie along the same linear trend in the log-log plot, and a line was fit to *all* of the data points. The relationship also appears to be independent of particle size in the diameter regime between 1 and 3 μm, since both sets of PSLs lie along the same trend. The least-square relationship for positive ions was

$$\sigma_y = 1.8883\langle y\rangle^{0.8976}, \tag{4.1}$$

where both y and σ_y are in units of mV·ns. The similar relationship for negative ions was

$$\sigma_y = 1.2883\langle y\rangle^{0.9366}. \tag{4.2}$$

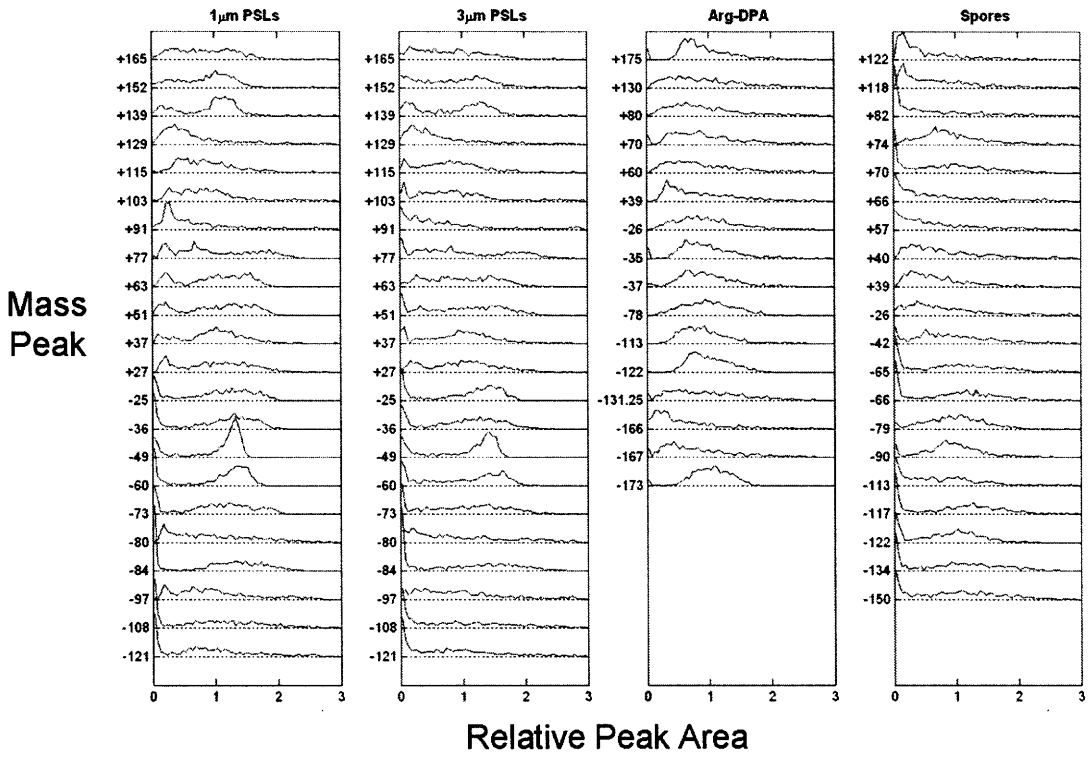

Figure 4-1: Relative peak area distributions for each mass peak studied. Mass peaks are labeled along the vertical axis, while the horizontal axis is a relative measure of peak area, in which the mean of each distribution was scaled to 1.

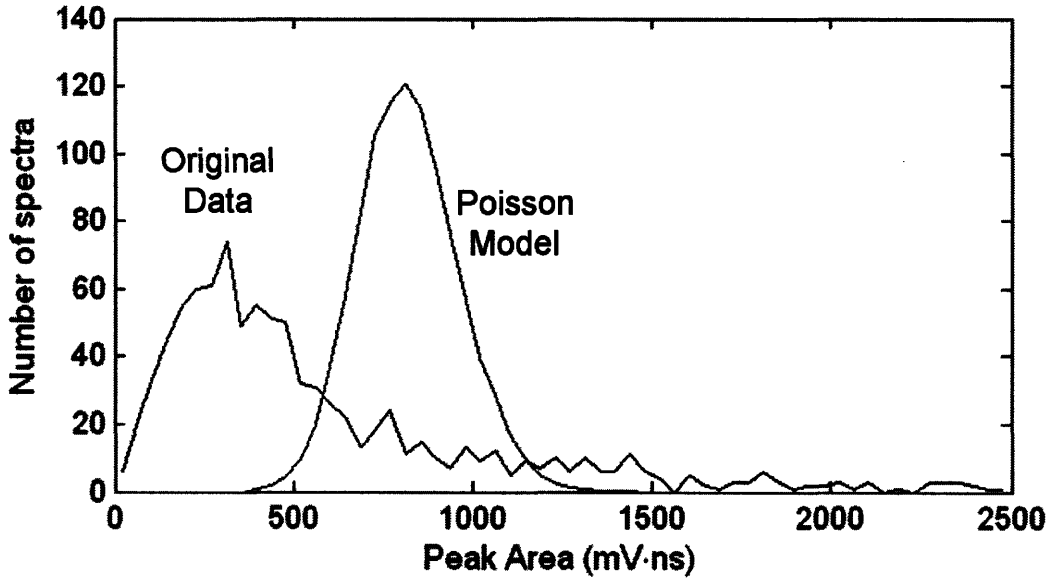

Figure 4-2: Peak area distribution for the +129 mass peak in the 1 μm PSL spectra (original data). Also shown is the average of twenty-five Monte Carlo simulations given a Poisson distribution for the number of ions generated per micro-particle. The mean and area of the two distributions are identical. For the Poisson model, the average of the two fitted curves in Figure 3-2b was used as the distribution for MCP gain.

While the fits are sublinear, they are quite different from the expected square root relationships predicted by Poisson statistics.

If neither the size nor the composition of a particle is responsible for the observed variation, then the source of this variation must be the LDI process or the detection process, the former of which I believe to be more likely. One potential cause of variation is spatial and temporal inhomogeneity in the laser profile. The average laser energy used to ionize a sample does affect the average peak area, but variations in pulse energy are relatively small. Spatial variations in laser fluence are more significant and would be expected to scale linearly with the laser energy. Another possibility is that the ionization events within a particle are highly correlated. Laser energy may not be uniformly absorbed throughout a particle, or a critical ion concentration may be required for a more significant ionization process to occur. In this case, one would expect significant deviations from a Poisson distribution in the peak area distributions for specific masses.

4.3 Variation between Spectra

The mass spectrum of each micro-particle was compared to the average (reference) spectrum of each of the four classes of micro-particles. In each comparison, only the peaks of the reference spectrum indicated in Figure 4-1 were considered. Two methods of comparison were used: the angles between the two multi-dimensional vectors, and the chi-square factors given by Equation 2.5, using the standard deviations from Equations 4.1 and 4.2.

Figure 4-4 shows the angular distributions, while Figure 4-5 shows the chi-square distributions. In both figures, each row represents a different reference spectrum, while each column represents the set of mass spectra being compared to the reference spectrum. Note that these distributions are not symmetric across the main diagonal, since diagonally opposite graphs represent different comparisons. In Figure 4-4, the percentages in each subplot are the percent of vectors that lie within 46 degrees (the angle used in Fergenson et al.) of the reference vector. Each sample was self-

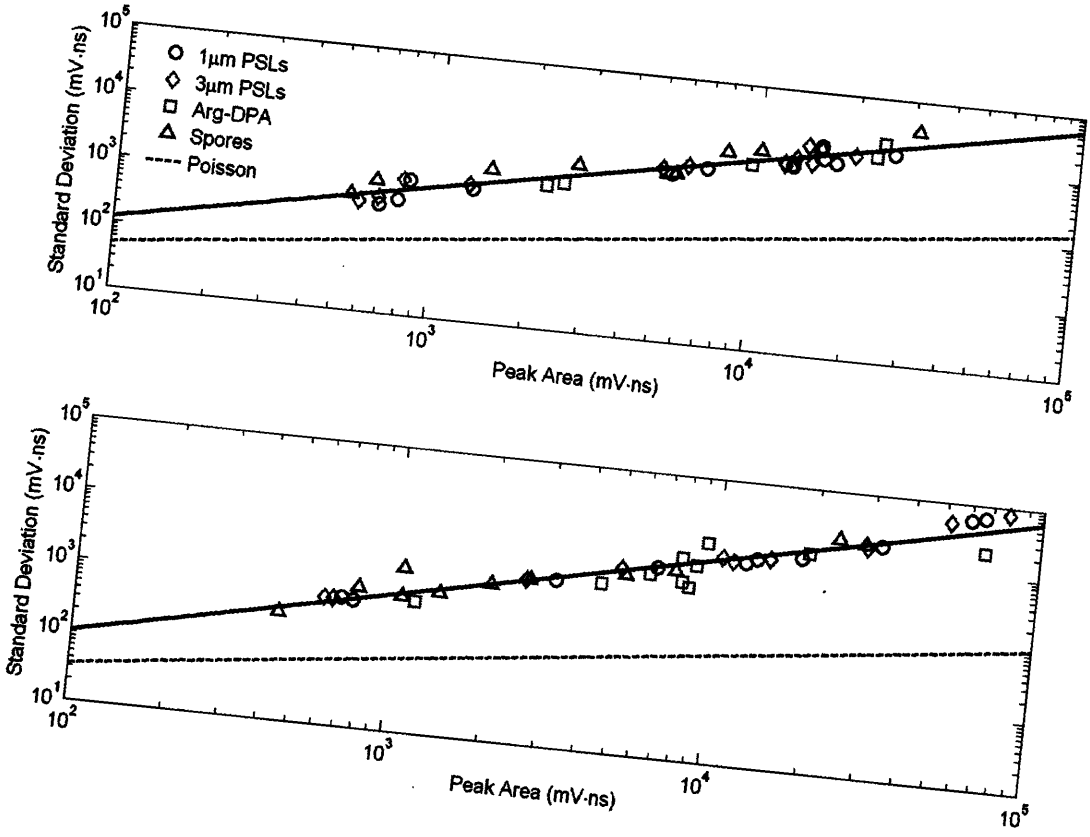

Figure 4-3: Variations in positive (top) and negative (bottom) mass peak areas for 1 μm and 3 μm PSLs, arginine-DPA, and bacterial spores. The dashed line indicates the theoretically derived lower limit, which assumes a Poisson distribution for ions generated and detected per particle. The solid line is a least-squares fit to the combined data of the four samples.

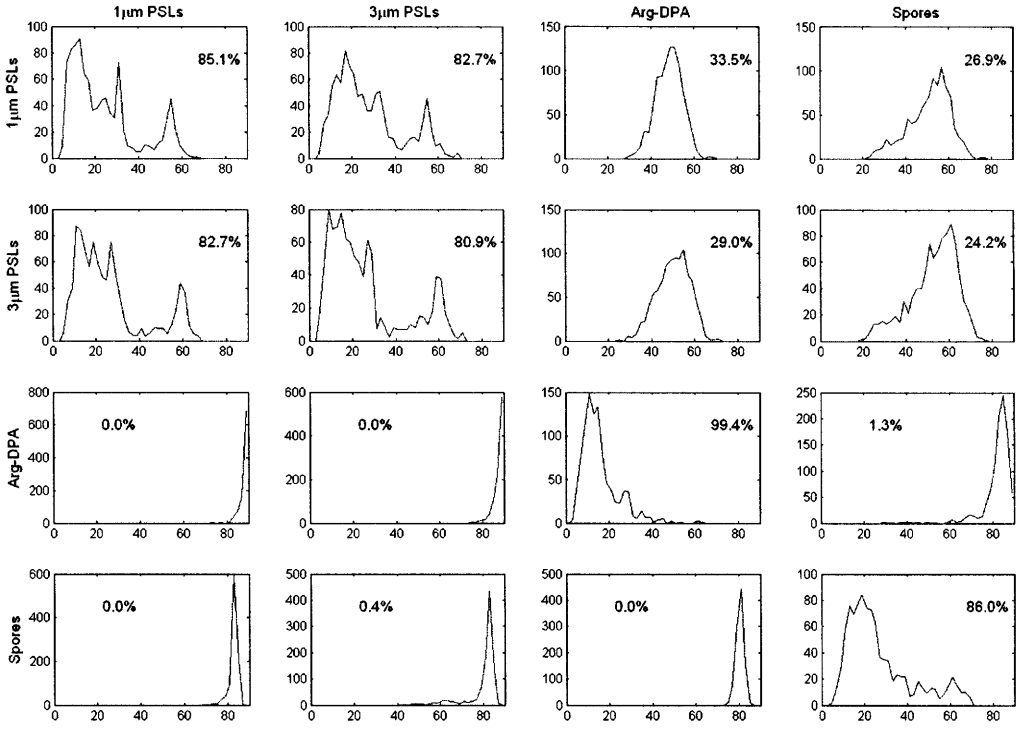

Figure 4-4: Pair-wise angular distributions. Each row uses a different reference vector. The horizontal axis of each graph is in units of degrees. Each subgraph represents approximately 1000 vectors being compared to a reference vector. The percentages within each subgraph are the percentages of vectors that lie within 46 degrees of the reference vector.

consistent (i.e., the percentages along the main diagonal are high), and there was agreement between the 1 and 3 μm PSL spheres (their off-diagonal percentages were also high). However, approximately 30 percent of both the arginine-DPA and spore samples were "confused" with the average spectra of 1 and 3 μm PSL spheres.

In Figure 4-5, the percentages of mass vectors with a chi-square value less than unity with respect to the reference vector are shown. It was found that more than 60 percent of the particles of each sample had a chi-square factor less than one with respect to that sample's average. Again, the spectra for both PSL samples were similar, while every other pair had very few chi-square factors less than one. The arginine-DPA and spore samples had chi-square values of approximately 1.5 with

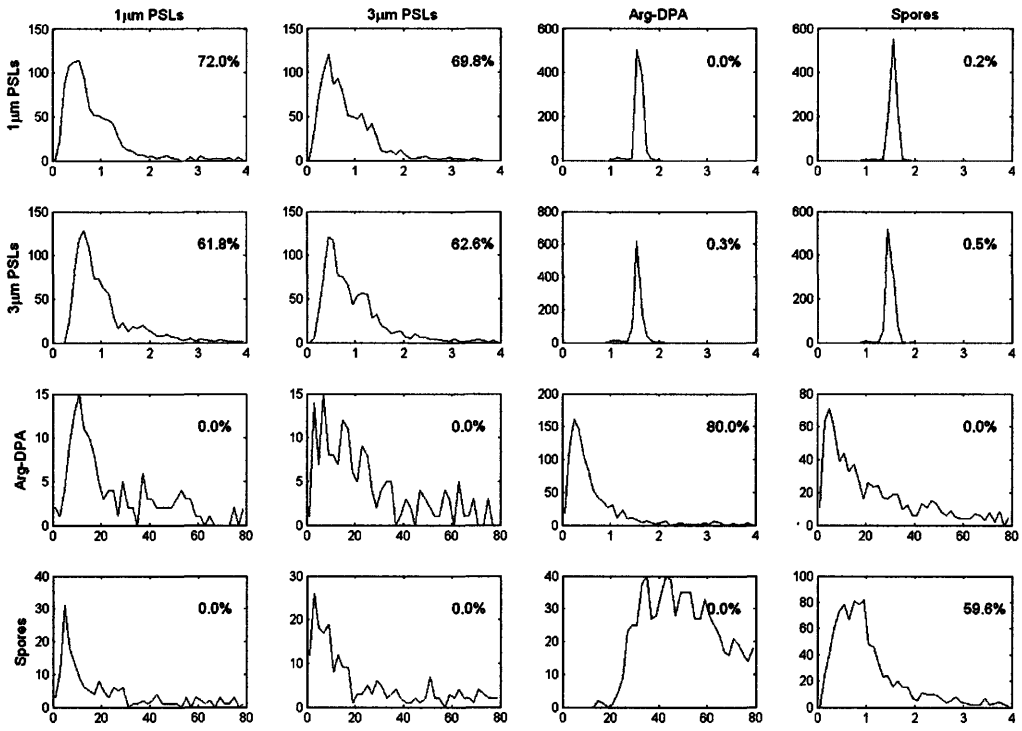

Figure 4-5: Pair-wise chi-square distributions. Each row uses a different reference vector ($\vec{Z}$ in Equation 5), while each column represents a set of 1000 vectors being compared to the reference vector ($\vec{Y}$ in Equation 5). In each subgraph, the horizontal axis indicates chi-square values The percentages within each graph are the percentages of spectra with reduced chi-squares less than unity.

respect to the PSL spheres, but these distributions in the upper right corner of Figure 4-5 were very narrow, and the micro-particles appear distinguishable via a chi-square test.

With the knowledge of the expected uncertainties in peak area measurements, I have demonstrated the viability of using specific peaks to calculate a chi-square factor to evaluate the similarity between two spectra. In this case, the vectors were not normalized. In the event that peak areas correlate strongly with some variable such as particles' aerodynamic diameters, a normalized reference spectrum (e.g., each vector is divided by particle volume) may be used, and Equation 2.5 may be modified accordingly.

Chapter 5

Conclusions

Mass spectrometry is a valuable tool for sample identification in a variety of scientific contexts, and is currently being explored for use in homeland security as a detection method for biological and chemical agents. When the phase space of molecules being probed is relatively small, such as for amino acids, identifying a molecule from its mass spectrum is a simple task. However, when the size of a phase space greatly exceeds the number of dimensions in the spectrum, greater precision is needed to determine the relative signal of each ionic species to correctly identify samples. The first goal of this study was to quantify the variations of these signals in SPAMS and to determine if such variations had statistical origins.

The single ion response of the microchannel plate was combined with Poisson counting statistics to generate a theoretical lower bound on peak area variation. I have shown that the standard deviations in peak area were approximately an order of magnitude larger than expected, and were remarkably consistent as a function of average peak area for 1 5m and 3 5m polystyrene latex spheres, arginine/dipicolinic acid micro-particles, and *Bacillus atrophaeus* spores. More specifically, it was found that the standard deviation in a peak's area was roughly proportional to the mean value of that area to the 0.9 power, with a constant of proportionality that was approximately the same for all particle diameters and compositions. I believe that the uniformity in the relationship between peak area mean and standard deviation was caused by variation in the laser desorption/ionization process that was independent

of the properties of the micro-particle being ionized.

While I believe that the precision limit has not been reached by the system in study, I have simultaneously developed a new method for quantitatively evaluating the similarity between mass spectra that makes use of the observed variations with a chi-square factor. I have also compared this chi-square method to the traditional angular separation method to demonstrate the usefulness of the chi-square method: spectra of micro-particles from the same samples were self-consistent, while those from different samples were not. Peak area variations of other single particle mass spectrometers may be similarly derived as they were in this study and used to generate chi-square tests for improved rapid particle identification. Ultimately, more advanced techniques involving learning algorithms and neural networks may be applied to organizing and comparing mass spectra. However, the chi-square method provides a first step in making better use of the available data.

References

[1] M. P. Sinha. Laser-induced volatilization and ionization of microparticles. *Review of Scientific Instruments*, 55(6):886–891, June 1984.

[2] S. C. Russell, G. Czerwieniec, C. Lebrilla, P. Steele, V. Riot, K. Coffee, M. Frank, and E. E. Gard. Achieving high detection sensitivity (14 zmol) of biomolecular ions in bioaerosol mass spectrometry. *Analytical Chemistry*, 77(15):4734–4741, August 2005.

[3] A. N. Martin, G. R. Farquar, E. E. Gard, M. Frank, and D. P. Fergenson. Identification of high explosives using single particle mass spectrometry.

[4] S. C. Russell, G. Czerwieniec, C. Lebrilla, P. Steele, V. Riot, K. Coffee, M. Frank, and E. E. Gard. Real-time analysis of individual atmospheric aerosol particles: Design and performace of a portable ATOFMS. *Analytical Chemistry*, 69(20):4083–4091, October 1997.

[5] P. T. Steele, A. Srivastava, M. R. Pitesky, D. P. Fergenson, H. J. Tobias, E. E. Gard, and M. Frank. Desorption/ionization fluence thresholds and improved mass spectral consistency measured using a flattop laser profile in the bioaerosol mass spectrometry of single *bacillus* endospores. *Analytical Chemistry*, 77(22):7448–7454, November 2005.

[6] R. J. Wenzel and K. A. Prather. Improvements in ion signal reproducibility obtained using a homogeneous laser beam for on-line laser desorption/ionization of single particles. *Rapid Communications in Mass Spectrometry*, 18(13):1525–1533, July 2004.

[7] D. B. Kane and M. V. Johnston. Size and composition biases on the detection of individual ultrafine particles by aerosol mass spectrometry. *Environmental Science and Technology*, 34(23):4887–4893, December 2000.

[8] S. C. Russell, G. Czerwieniec, C. Lebrilla, H. Tobias, D. P. Fergenson, P. Steele, M. Pitesky, J. Horn, A. Srivastava, M. Frank, and E. E. Gard. Toward understanding the ionization of biomarkers from micrometer particles by bio-aerosol mass spectrometry. *Journal of the American Society for Mass Spectrometry*, 15(6):900–909, June 2004.

[9] F. Drewnick, S. S. Hings, P. DeCarlo, J. T. Jayne, M. Gonin, K. Fuhrer, S. Weimer, J. L. Jimenez, K. L. Demerjian, S. Borrmann, and D. R. Worsnop. A new time-of-flight aerosol mass spectrometer (TOF-AMS) – instrument description and first field deployment. *Aerosol Science and Technology*, 39(7):637–658, July 2005.

[10] W. A. Harris, P. T. A. Reilly, and W. B. Whitten. MALDI of individual biomolecule-containing airborne particles in an ion trap mass spectrometer. *Analytical Chemistry*, 77(13):4042–4050, July 2006.

[11] I. Cohen, R. Gola, and S. R. Rotman. Applying branching processes theory for building a statistical model for scanning electron microscope signals. *Optical Engineering*, 39(1):254–259, January 2000.

[12] B. A. Mansoori and M. V. Johnston. Matrix-assisted laser desorption/ionization of size- and composition-selected aerosol particles. *Analytical Chemistry*, 68(20):3595–3601, October 1996.

[13] D. P. Fergenson, M. E. Pitesky, H. J. Tobias, P. T. Steele, G. A. Czerwieniec, S. C. Russell, C. B. Lebrilla, J. M. Horn, K. R. Coffee, A. Srivastava, S. P. Pillai, M.-T. P. Shih, H. L. Hall, A. J. Ramponi, J. T. Chang, R. G. Langlois, P. L. Estacio, R. T. Hadley, M. Frank, and E. E. Gard. Reagentless detection and classification of individual bioaerosol particles in seconds. *Analytical Chemistry*, 76(2):373–378, January 2004.

[14] S. E. Stein and D. R. Scott. Optimization and testing of mass spectral library search algorithms for compound identification. *Journal of the American Society for Mass Spectrometry*, 5(9):859–866, September 1994.

[15] S. Coeck, M. Beck, B. Delaure, V. V. Golovko, M. Herbane, A. Lindroth, S. Kopecky, V. Y. Kozlov, I. S. Kraev, T. Phalet, and N. Severijns. Microchannel plate response to high-intensity ion bunches. *Nuclear Instruments and Methods in Physics Research A*, 557(2):516–522, February 2006.

[16] K. Furuya and Y. Hatano. Pulse-height distribution of output signals in positive ion detection by a microchannel plate. *International Journal of Mass Spectrometry*, 218(3):237–243, July 2002.

[17] J. Axelsson, C. T. Reimann, and B. U. R. Sundqvist. Size and composition biases on the detection of individual ultrafine particles by aerosol mass spectrometry. *International Journal of Mass Spectrometry and Ion Processes*, 133(2):141–155, May 1994.

[18] K. L. Hunter and R. W. Stresau. Influence of detector pulse height distribution on abundance accuracy in TOF-MS. In *10th Sanibel Conference on Mass Spectrometry*, 1998.